Asian Journal of Chemistry; Vol. 38, No. 4 (2026), 1073-1086
ASIAN JOURNAL OF CHEMISTRY
https://doi.org/10.14233/ajchem.2026.35527

Ce doped ZnO Catalyst for Degradation of Triethylamine under Solar Light: A Comparative Study of Sol-Gel and Co-precipitation Synthesis

NETAJI P. MALI[1,*], AMOL S. BHOSALE[1], SHAILA B. DHOTRE[1], SHRIKANT P. TAKLE[1], RAVINDRA U. MENE[2] and NAMDEO N. BHUJBAL[1]

[1]Department of Chemistry, Annasaheb Magar Mahavidyalaya, Hadapsar, Pune-411028, India
[2]Department of Physics, Annasaheb Magar Mahavidyalaya, Hadapsar, Pune-411028, India

*Corresponding author: E-mail: malinetaji@gmail.com

Received: 27 December 2025 *Accepted*: 16 March 2026 *Published online*: 8 April 2026 AJC-22331

Zinc oxide (ZnO) and cerium-doped ZnO (Ce-ZnO) nanoparticles were produced through sol-gel (SG) and coprecipitation (CPPT) techniques. The impact of cerium doping, ranging from 1% to 5% on the structural, morphological, optical, photoluminescence and photocatalytic characteristics was examined. X-ray diffraction analysis suggested a well-defined hexagonal wurtzite structure. The largest crystallite sizes were 56 nm for 2% Ce-ZnO (SG) and 70 nm for 3% Ce-ZnO (CPPT). The morphology of the particles was affected by the cerium concentration. FESEM, EDS mapping and HR-TEM indicates a uniform distribution of cerium and a hexagonal shape. UV-DRS analysis indicated strong absorption below 450 nm with a reduction in bandgap from 3.13 eV of undoped ZnO to 2.32 eV (SG) and 2.37 eV (CPPT) of Ce-ZnO, whereas photoluminescence showed a blue-shifted emission around 427-425 nm. TGA implies the thermal stability upto above 680 ºC. Ce-ZnO achieved up to 98% (SG) and 85% (CPPT) photodegradation of triethylamine (TEA) under sunlight as monitored by UV-Vis spectroscopy and TOC analysis.

Keywords: Sol-gel, Co-precipitation, Amine degradation, Triethylamine.

INTRODUCTION

The rapid rise in industrialisation coupled with an increasing population and environmental pollution has emerged as a significant global issue [1]. Worldwide, tackling pollution prevention and reduction has emerged as a significant challenge. Every day, a substantial volume of wastewater from amine industries released into aquatic environments. One of the major pollutant compounds is amine and their derivatives. The amines found in the wastewater from various industrial effluents exhibit cytotoxic, neurogenic, teratogenic and carcinogenic effects [2]. There are different techniques for removal of these amines from wastewaters such as filtration, ionisation, ion-exchange, adsorption, degradation, *etc*. involved [3,4]. Among these methods, photocatalytic degradation is a highly effective technique, in which various nanomaterials, including zinc oxide (ZnO), play an important role in the degradation process. ZnO is an important semiconductor material with a direct band gap of 3.37 eV and a notable exciton binding energy of 60 MeV at room temperature [5,6]. It is attracting considerable research interest due to its fascinating electrical, photocatalytic, opto-electrical and magnetic properties [7-9].

Releasing harmful chemicals into water bodies has led to a worldwide issue of water pollution. Amines have garnered considerable attention due to their extensive use in various industries such as amine manufacturing, pharmaceuticals, paints, pesticides, printing, textiles, paper and plastics [10-12]. Addressing this problem can enhance both human living conditions and aquatic ecosystems. At present, advanced semiconductor photocatalysis is considered a promising approach for addressing water pollution and energy challenges due to its cost-effectiveness, environmental friendliness, reusability and high efficiency in pollutant removal [13-15]. Semiconductor metal oxide nano-photocatalysts including ZnO, SnO_2, Bi_2O_3 and TiO_2 are extensively employed to remove toxic substances from wastewater under various light sources due to their excellent chemical stability and capability to oxidize low concentrations of organic pollutants [16-19].

ZnO nanoparticles are widely used in commercial products and their effectiveness and toxicity are continuously moni-

This is an open access journal, and articles are distributed under the terms of the Attribution 4.0 International (CC BY 4.0) License. This license lets others distribute, remix, tweak, and build upon your work, even commercially, as long as they credit the author for the original creation. You must give appropriate credit, provide a link to the license, and indicate if changes were made.

tored, although slight toxicity has been reported at higher concentrations [20]. As an n-type semiconductor oxide, ZnO is cost-effective, relatively non-toxic and efficient for the degradation of organic pollutants [21,22]; however, its application is limited to UV light utilization, which constitutes only about 5% of the solar spectrum, resulting in low solar energy utilization.

Several studies have found enhancements in the properties of ZnO nanoparticles, specifically regarding their particle size, bandgap and surface area [23]. Moreover, the rapid recombination of photo-generated electron-hole pairs [$(e^-)/(h^+)$ pairs] in ZnO leads to a low quantum yield, negatively impacting its photocatalytic efficiency and significantly restricting its application [24-26]. Various strategies have been implemented to reduce recombination, enhance light absorption and improve its photocatalytic performance, including semiconductor recombination [27,28], precious metal deposition [29-31] and cation modification. ZnO enhanced with rare earth ions has assembled significant attention in doping strategies [32].

Rare earth ions, known for their unique 4*f*-electron shells and complex energy levels, serve as activator centres in various host materials due to their narrow fluorescence bands and high efficiency, making them popular in displays, biomedical applications, lighting and lasers. Numerous studies have explored the incorporation of transition metals like In, Sb, Ag and Co as dopants in semiconductors to tailor the properties of ZnO [33-36]. In contrast, there has been less research focused on lanthanide elements. Lanthanides including Ce, La, Sm and Nd have been utilised as dopants in semiconductors [37,38] resulting in the creation of surface defects. Among these, cerium has garnered considerable interest due to its distinctive characteristics such as (i) the ability to create highly unstable oxygen vacancies with relatively high mobility of bulk oxygen species and (ii) its role as an electron trap that prevents the recombination of photogenerated charge carriers. Recent research has indicates enhancements in the photocatalytic activity of ZnO when doped with cerium [39-41]. Ce-ZnO with hexagonal, rod shaped ZnO offer good conductivity, a large surface area and high adsorption capacity [42-45] making them ideal for supporting photocatalysts due to their low UV light transmissivity and ability to effectively trap and transfer photo-induced electrons [46,47]. Thus, to conserve energy and cut costs, it is crucial to create new eco-friendly visible light photocatalysts for amine wastewater treatment. In this research, cerium doped ZnO materials with varying Ce contents (Ce-ZnO) were prepared by SG and CPPT methods. The synthesised material was analysed using XRD, FESEM, HR-TEM, UV-DRS, photoluminescence (PL) and XPS. The study thoroughly examined the photocatalytic performance of ZnO and Ce-ZnO in the visible light for degradation of triethylamine.

EXPERIMENTAL

For synthesis, zinc nitrate hexahydrate $Zn(NO_3)_2{\cdot}6H_2O$, cerium nitrate hexahydrate $Ce(NO_3)_3{\cdot}6H_2O$, NaOH were used. All the material was AR grade, received from Merck and used as received. Milli-Q water (conductivity 0.06 μS/cm, Q-Pad filter system) was used throughout the process of synthesis. Triethylamine was used as pollutant for degradation performance.

Synthesis of ZnO and Ce-ZnO NPs by sol-gel method: ZnO nanoparticles were synthesized by preparing a 0.5 M $Zn(NO_3)_2$ solution in Milli-Q water, followed by magnetic stirring for 1 h to obtain a homogeneous solution. Subsequently, 5% NaOH solution was added dropwise to adjust the pH to 8, resulting in the formation of a thick aerogel, which was further stirred for 12 h at 60 ºC to obtain a uniform gel. The gel was dried under an IR lamp at 120 ºC and calcined at 700 ºC to obtain white-coloured ZnO nanoparticle powder. For Ce–ZnO synthesis, an equivalent amount of $Ce(NO_3)_3{\cdot}6H_2O$ was dissolved in Milli-Q water, stirred for 1 h, mixed with the $Zn(NO_3)_2$ solution, and stirred for an additional 0.5 h; the remaining procedure was identical, yielding 1-5% Ce-doped ZnO nanoparticles.

Synthesis of ZnO and Ce-ZnO NPs by co-precipitation method: For CPPT synthesis, 1 M $Zn(NO_3)_2{\cdot}6H_2O$ solution was prepared. In a separate beaker, an equivalent amount of $Ce(NO_3)_3{\cdot}6H_2O$ was dissolved in Milli-Q water and stirred for 1 h. The two solutions were then mixed and stirred for 0.5 h, followed by dropwise addition of 5% NaOH to adjust the pH to 12, resulting in precipitation. The mixture was further stirred for 12 h at 60 ºC and allowed to settle, after which the supernatant was decanted and the precipitate was washed 3-4 times with Milli-Q water. The obtained precipitates were dried under an IR lamp and annealed at 700 ºC to obtain pure and Ce-ZnO nanoparticle powders, and by this method, 1-5% Ce-doped ZnO NPs were synthesized. The flow diagram for the synthesis of Ce-doped ZnO NPs is shown in Fig. 1.

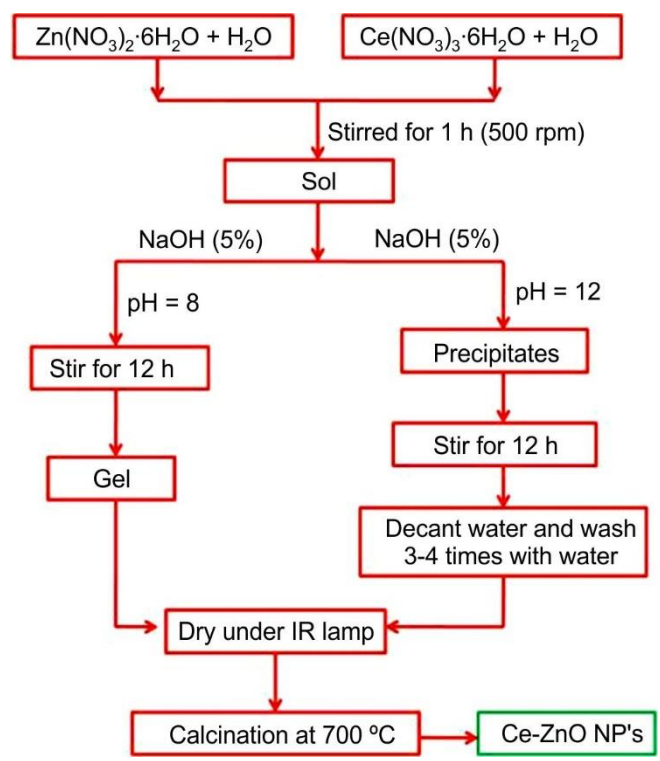

Fig. 1. Flow diagram for synthesis of Ce-ZnO NPs by SG and CPPT methods

Characterisation: The crystallographic analysis of the synthesised sample was conducted using a Rigaku Ultima IV X-Ray Diffractometer, employing Cu*K*α radiation (λ = 1.5406 Å) as source. Diffraction data were gathered within a 2θ range

of 20 to 80º at a scanning speed of 10 ºC per min. For examining the elemental composition and morphology of the catalysts, a field-emission scanning electron microscope (FE-SEM, FEI Nova Nano SEM 450) was used. The distribution of cerium in ZnO was assessed through energy dispersive X-ray spectroscopy (EDX), complemented by essential mapping studies (EDS, Bruker X-Flash 6I30). High resolution transmission electron microscopy (HR-TEM) images were captured using a PHILIPS CM200 field emission transmission electron microscope (FE-TEM), operating at voltages between 20 and 200 kV with a resolution of 2.4 Å and selected area electron diffraction (SAED) patterns were also recorded. The optical characteristics of the sample were evaluated using a Perkin-Elmer UV-visible spectrophotometer. Raman spectroscopy was used to study the vibrational properties and crystalline structure of undoped and doped ZnO using a HORIBA Scientific Raman spectrometer with a 532 nm excitation laser. The uncalcined powders prepared by sol-gel (SG) and co-precipitation (CPPT) methods were thermally analysed using an SDT Q600 V20.9 Build 20 analyzer from room temperature to 1000 ºC at a heating rate of 10 ºC/min, with α-Al_2O_3 as the reference.

RESULTS AND DISCUSSION

Thermal studies: Thermogravimetric analysis (TGA) was performed on the synthesised ZnO NPs. As shown in Fig. 2, a slight weight loss of 3.88% was observed around 120 ºC, followed by a 12.18% reduction at 187 ºC due to evaporation of water. Another weight loss of 21.17% occurred up to 161 ºC, attributed to the removal of certain oxides, while a major weight loss of 36.82% between 161 ºC and 680 ºC corresponded to the decomposition of organic and inorganic groups; beyond 680 ºC, no significant changes were observed.

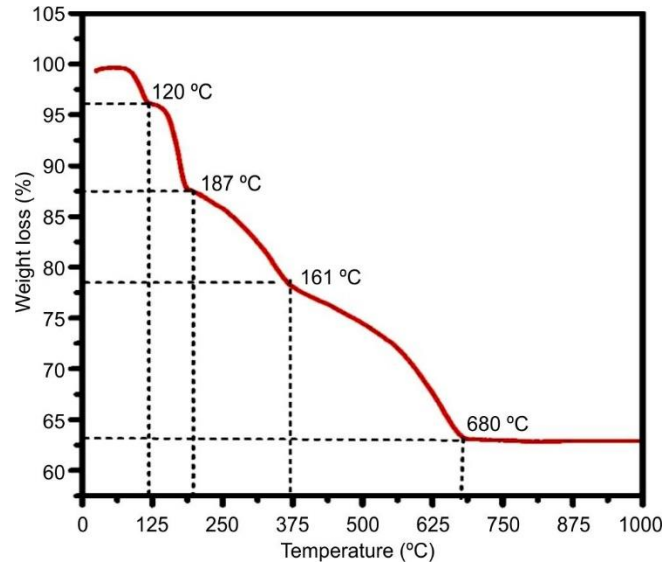

Fig. 2. Thermogravimetric curve for 3% Ce-ZnO NPs

XRD studies: The crystal structure and phase composition of undoped and 1%-5% Ce doped ZnO nanoparticles synthesised by SG and CPPT methods were investigated using X-ray diffraction (XRD) as shown in Fig. 3. All diffraction peaks can be indexed to the hexagonal wurtzite phase structure of ZnO indicating good crystallinity of the powdered samples. At lower concentrations of Ce, no peaks associated

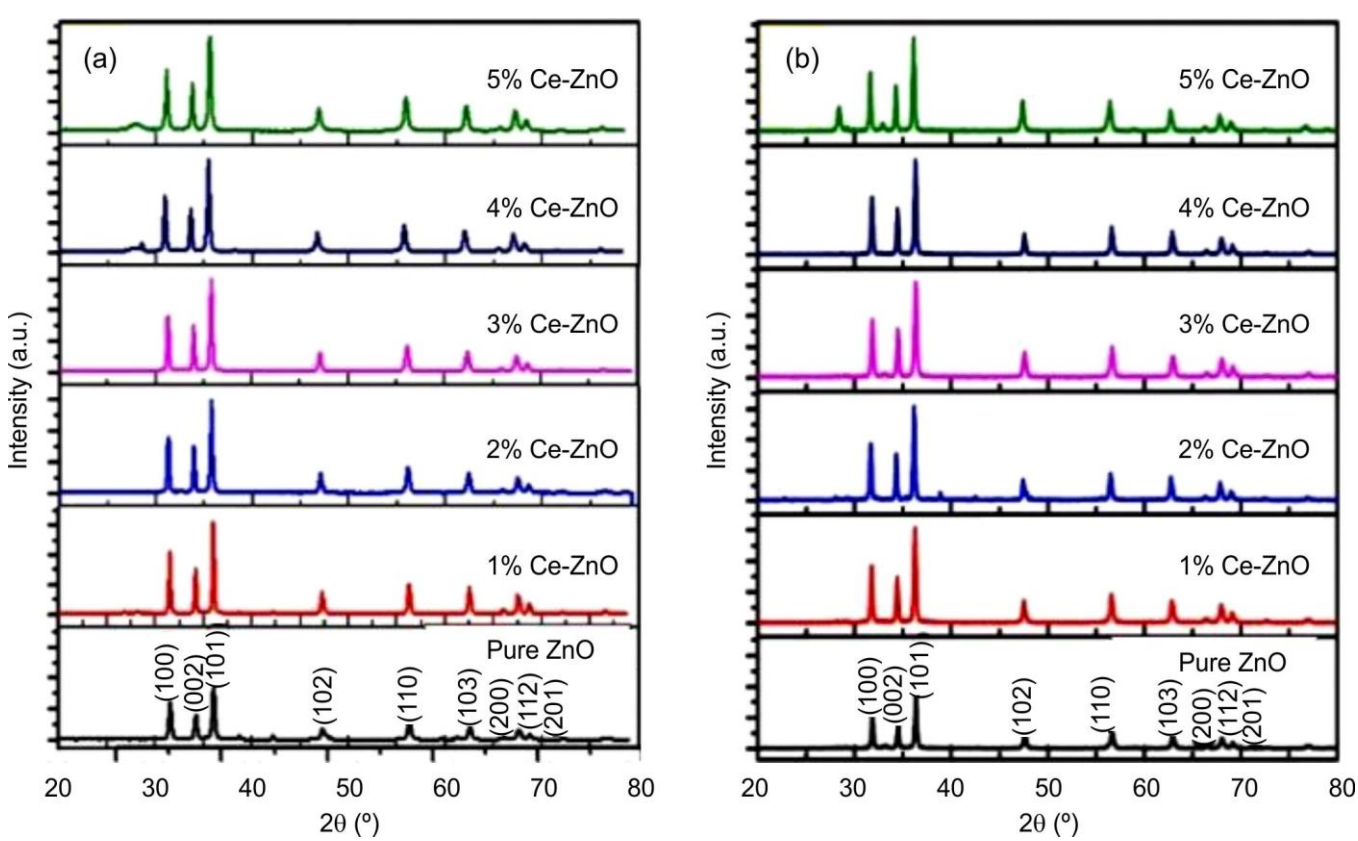

Fig. 3. XRD pattern for ZnO and 1% to 5% Ce-ZnO NPs for (a) SG and (b) CPPT methods

with impurities were detected indicating the successful formation of phase-pure ZnO. At higher doping level of Ce, the peak at 28.34º is imputed to (111) plane for cubic crystal structure CeO_2 [48-50]. Also, systematic shifting of main diffraction peaks of ZnO to the lower angles indicates the lattice distortion and partial Ce incorporation due to difference in ionic radii of Ce^{3+}/Ce^{4+} and Zn^{2+}.This suggest that excess Ce may not fully substitute Zn^{2+} in the ZnO lattice but partially segregates as a secondary phase. The average crystalline size (d) was estimated using the Scherrer formula [51] and summarised in Table-1.

$$D = \frac{0.9k}{\beta \cos\theta}$$

exhibited minor variation as the Ce content increased while samples derived from CPPT maintained relatively stable crystallite sizes. This difference can be attributed to variations in the nucleation and growth mechanisms, which arise from the larger ionic radii of Ce^{3+} (0.102 nm) and Ce^{4+} (0.092 nm) compared to Zn^{2+} (0.074 nm), as reported by other researchers [52-55]. Therefore, it is challenging for Ce^{3+} and Ce^{4+} to invade into the ZnO crystal lattice and replace Zn^{2+}. The systematic shift in main diffraction peaks of ZnO to the lower angle at higher Ce level in Ce-ZnO for both the synthesis method indicated the lattice distortion and partial Ce incorporation due to difference in ionic radii of Ce^{3+}/Ce^{4+} and Zn^{2+} [56,57]. Based on these observations, the SG method is superior to the CPPT method for synthesising ZnO nanoparticles with precise structural tuning.

FE-SEM studies: Fig. 4a-b shows SEM images and its EDS pattern for ZnO and (c and d) for 3% Ce-ZnO for SG method. Also Fig. 5a-b shows SEM images and its EDS pattern

TABLE-1
CRYSTALLITE SIZE (CS) AND FWHM FOR NANOPARTICLES PREPARED BY SG AND CPPT METHODS

Method	Parameters	ZnO	1% Ce-ZnO	2% Ce-ZnO	3% Ce-ZnO	4% Ce-ZnO	5% Ce-ZnO
Sol-gel	CS (nm)	29.32	26.6	28.8	27.83	25.23	28.21
	FWHM (º)	32.29	0.33	0.328	0.326	0.360	0.323
CPPT	CS (nm)	31.77	31.03	33.43	33.66	33.08	30.56
	FWHM (º)	0.320	0.277	0.272	0.277	0.280	0.305

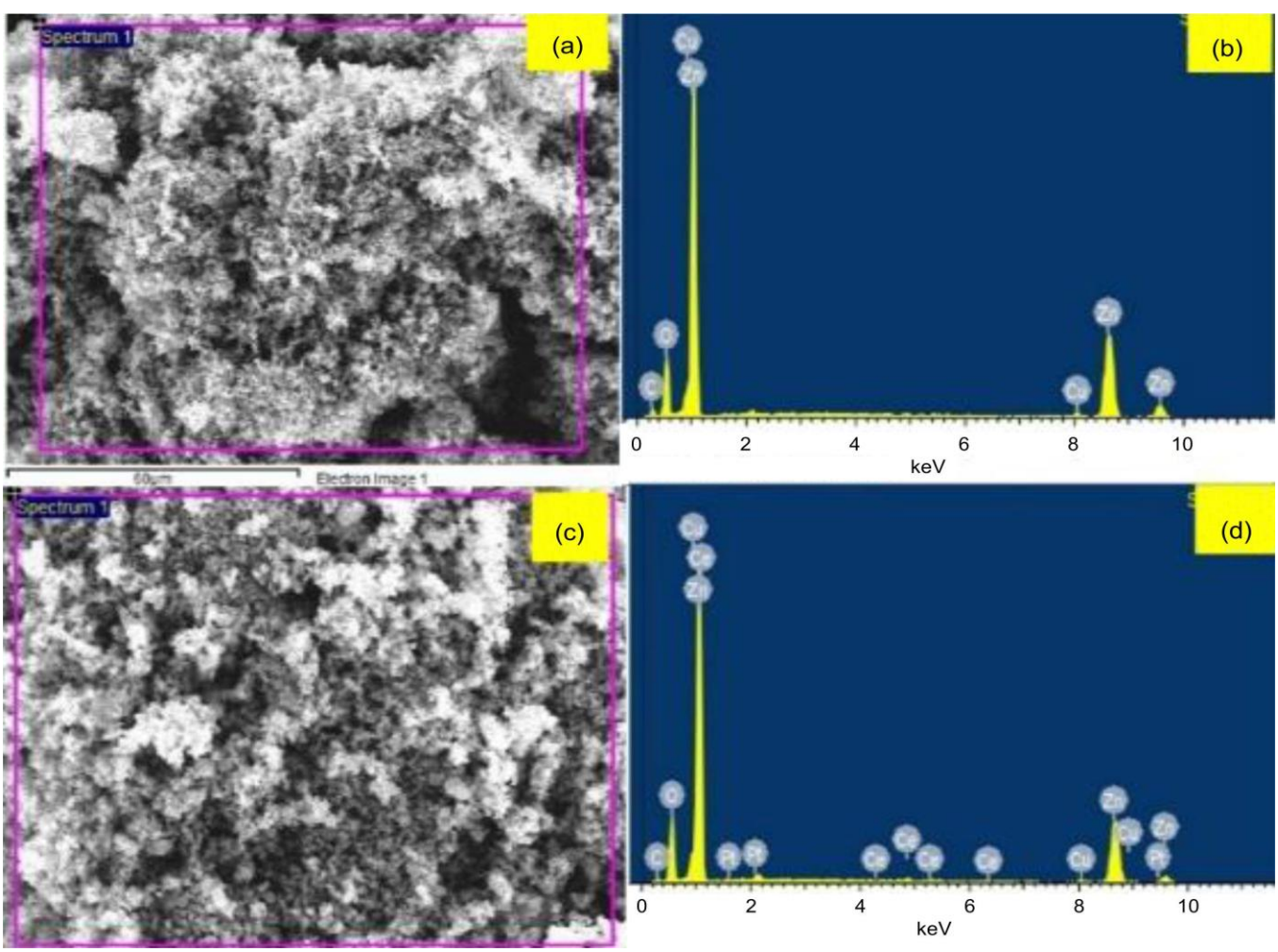

Fig. 4. SEM images and EDS pattern (a and b) for ZnO and (c and d) for 3% Ce-ZnO by SG method

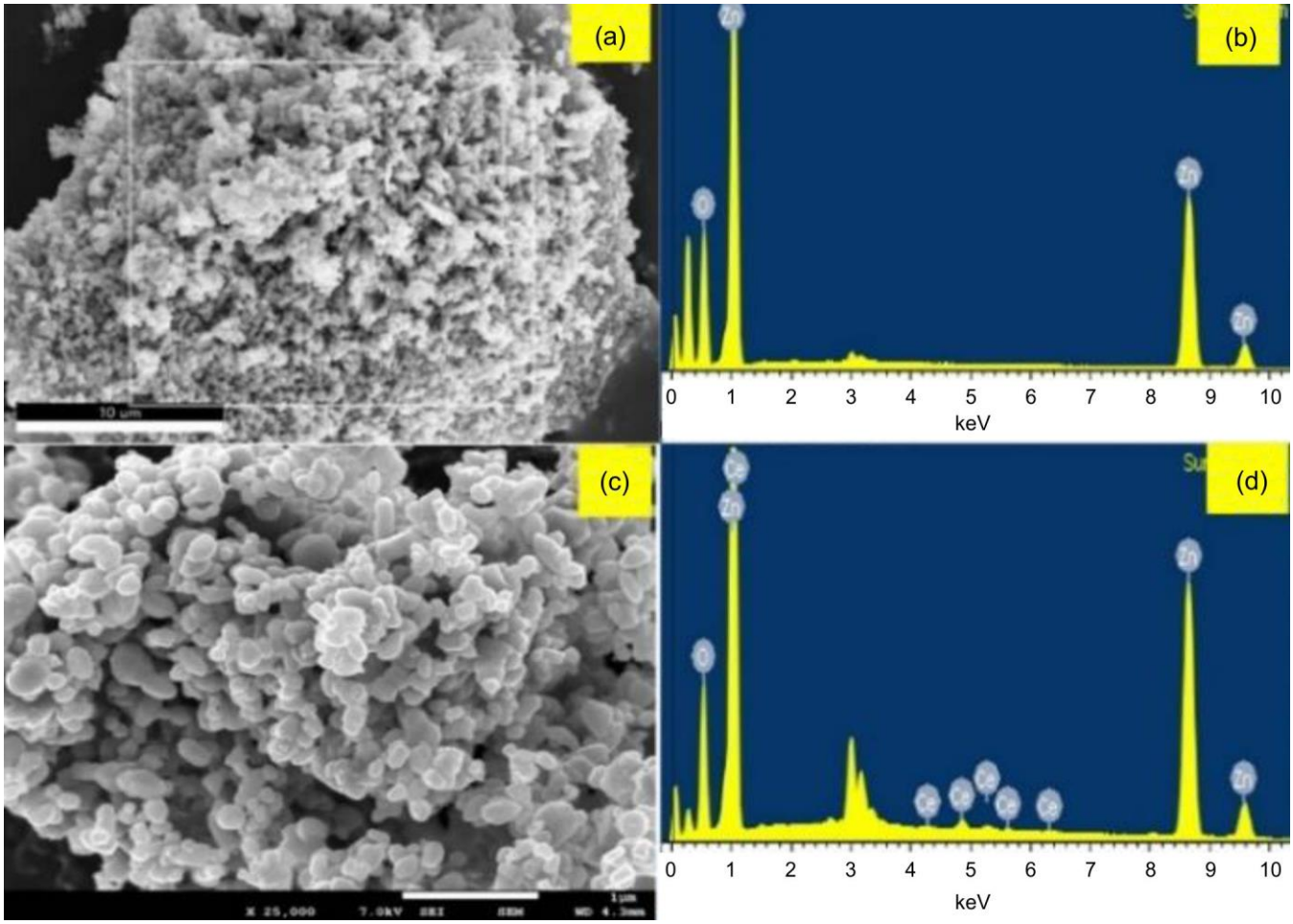

Fig. 5. SEM image (a) and EDS spectra (b) for ZnO and (c and d) for 3% Ce-ZnO by CPPT method

for ZnO and (c and d) 3% Ce-ZnO for CPPT method. The average size for SG is 63.74 nm and 86.12 nm for CPPT for 3% Ce-ZnO. This image shows that synthesised particles by both methods are uniform distribution and exhibit good interconnectivity between particles. A distinguished difference in morphology is observed for ZnO and Ce-ZnO. As light reduction in particle size and improved uniformity were observed for SG-derived samples compared to CPPT samples consistent with the crystallite size trends obtained from XRD analysis.

The EDS elemental mapping images of 3% Ce-ZnO (Fig. 6) confirm the presence and homogeneous distribution of Zn, Ce and O throughout the sample. The individual maps show Zn (b), Ce (c) and O (d), indicating successful incorporation of cerium into the ZnO lattice without noticeable elemental segregation [52].

HR-TEM studies: The particle structure, size distribution and crystallinity of synthesised catalyst were analysed by HR-TEM technique. The incorporation of Ce^{3+} in ZnO lattice is identified by HRTEM images, their SAED pattern and interplanar distance for ZnO and 3% Ce-ZnO prepared by SG and CPPT method shown in Fig. 7a-f. These images affirm the presence of a bulk quantity of hexagonal small Ce-ZnO nanoparticles distribution. These nanoparticles are closely packed at the nanometre scale and the average particle sizes

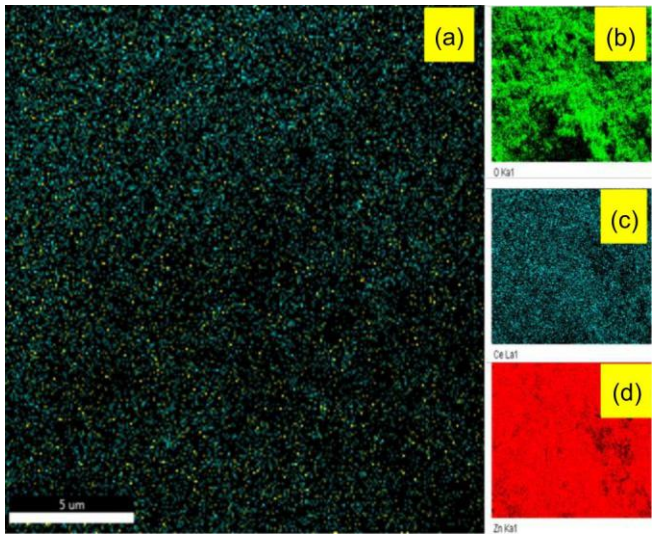

Fig. 6. EDS mapping images (a) 3%Ce-ZnO (b) oxygen (c) cerium and (d) zinc

estimated from TEM images is 67 nm which is in good agreement with the crystallite sizes obtained from XRD indicating that the particles are predominantly single crystalline [52]. The SAED pattern is depicted in Fig. 7c (SG) and 7d (CPPT) for Ce-ZnO nanoparticles. SAED patterns show well-defined

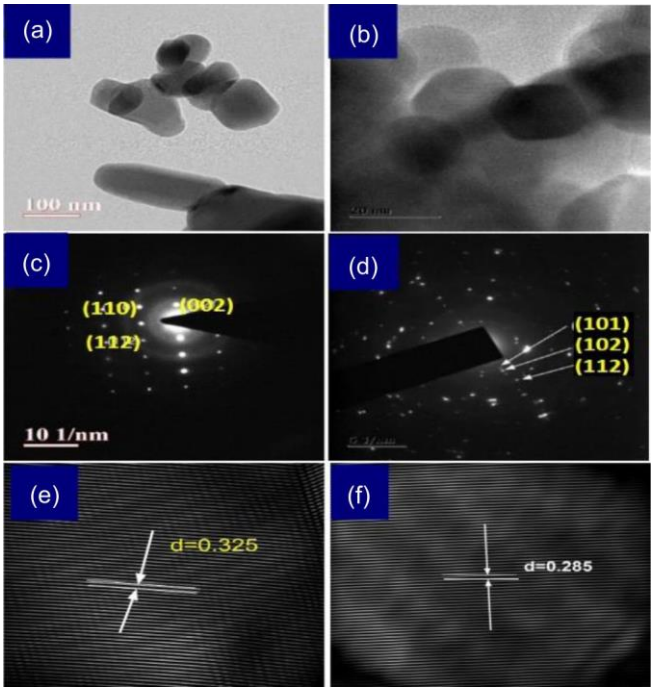

Fig. 7. (a and b) TEM images for SG and CPPT, (c and d) SAED pattern of 3% Ce-ZnO for SG and CPPT, (e and f) lattice image for SG and CPPT methods

concentric rings further analysed the polycrystalline nature of the nanoparticles [22]. The *d*-spacing (002) lattice planes for 3% Ce-ZnO synthesised by SG and CPPT methods is found to be 0.325 nm and 0.285 nm, respectively (Fig. 7e-f), which suggest that the Ce-doped ZnO nanoparticles grew along [001] direction [53].

XPS analysis: Full scan XPS spectra of ZnO and 3% Ce-ZnO is shown in Fig. 8. The high-resolution XPS of the Zn2*p* region for 3% Ce-ZnO reveals peaks at 1021.75 and 1045.95 eV (Fig. 8c) [54], which are slightly shifted to higher binding energies compared to ZnO (1018.75 and 1043.95 eV). Fig. 8d presents the XPS of the O1*s* region for 3% Ce-ZnO which is asymmetric and consists of two components: a low-intensity peak at 531.11eV and a prominent peak at 529.52 eV. The former is linked to photoemission in O^{2-} ions with the valence oxygen, such as surface-adsorbed oxygen and O [58]. Consequently, the O1*s* peak of 3% Ce-ZnO is asymmetric with the 531.11eV components being more pronounced than in ZnO indicating a higher number of oxygen vacancies in 3% Ce-ZnO. The high-resolution XPS scan of the Ce3*d* region shows prominent peaks at 880.6 and 898 eV, assigned to the $3d_{5/2}$ state of Ce^{4+} ions [57] and peaks at 903.76, 907.2 and 916.3 eV assigned to the $3d_{3/2}$ state of Ce^{3+} ions on the ZnO surface [59] (Fig. 8b). These Ce^{3+} dopant ions can capture photogenerated electrons and inhibit electron–hole recombination.

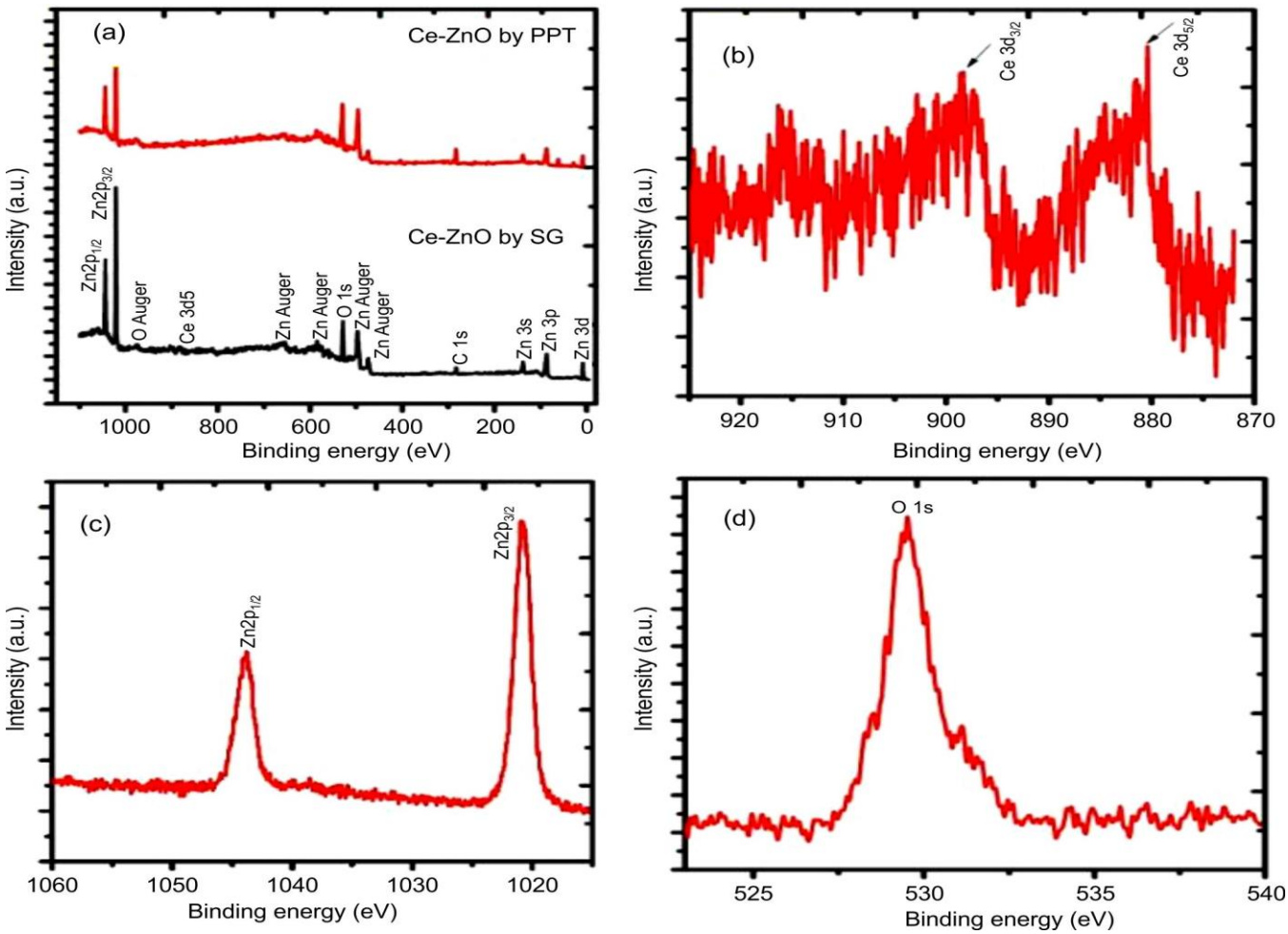

Fig. 8. XPS spectra of 3% Ce-ZnO NPs (a) survey scan, (b) Ce3d, (c) Zn 2p and (d) O 1*s* spectrum

UV-DRS studies: All samples were analysed by UV-DRS to examine the optical properties of synthesised samples. Fig. 9a-b illustrates typical diffuse reflectance spectra for Ce-doped ZnO by SG and CPPT techniques, respectively. The optical band gap values were determined using Tauc plots (Fig. 9c-d) with the assumption of a direct allowed transition. Upon Ce doping, the band gap slightly decreases for both synthesis methods due to the defect states and localized energy levels introduced by Ce ions along with associated oxygen vacancies in SG and CPPT samples, and the band gap values of Ce-doped ZnO with varying Ce contents for both methods are summarized in Table-2. Based on these results, it is found that Ce doping effectively narrows the band gap of ZnO enhancing visible-light absorption which is beneficial for the photocatalytic activity.

Raman spectral studies: Raman spectroscopy was used to examine the vibrational characteristics and lattice disorder of ZnO and Ce-doped ZnO nanoparticles synthesised by SG

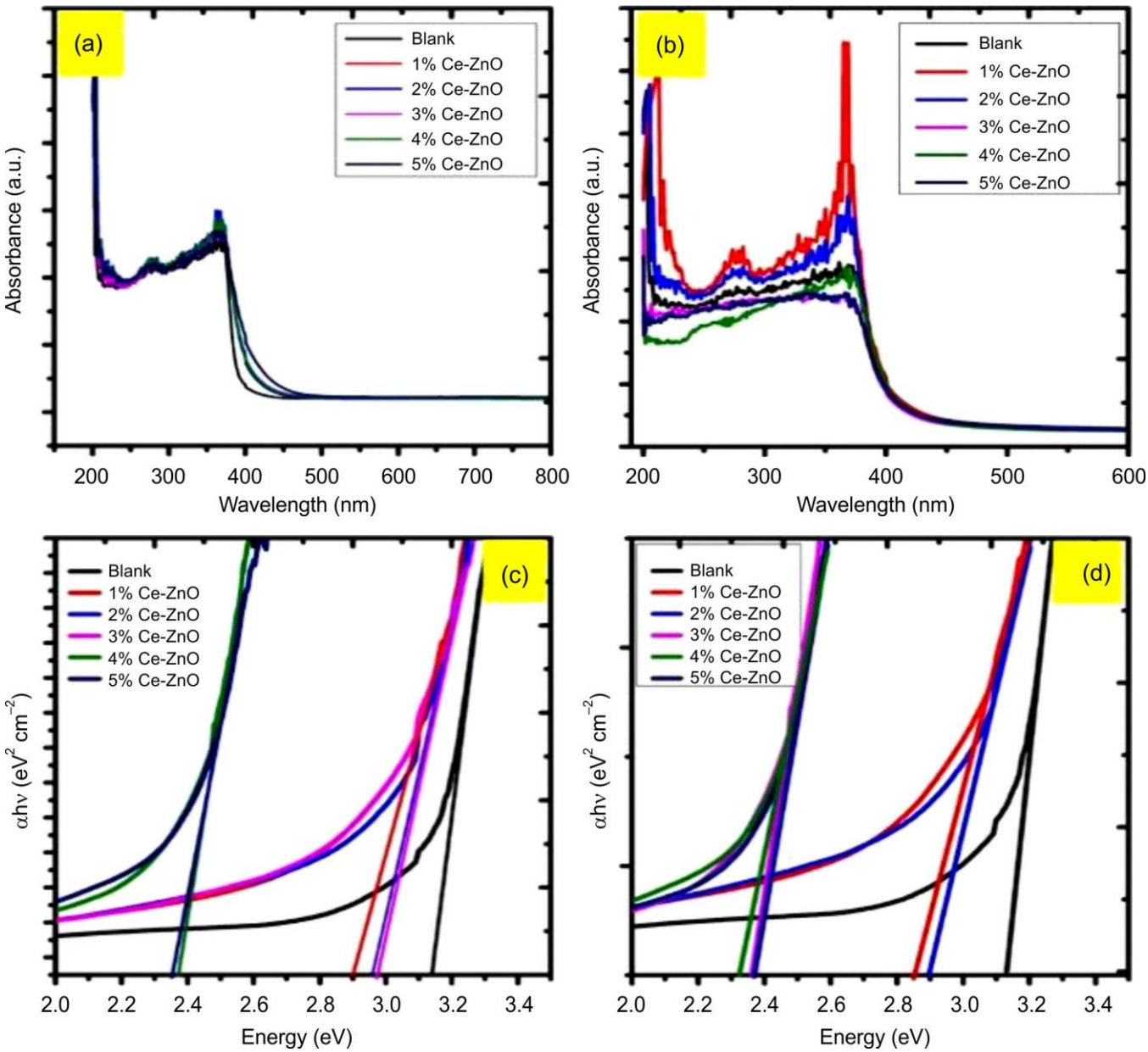

Fig. 9. Absorption spectra for (a) SG (b) CPPT method; Tauc plot for (c) SG (d) CPPT method for ZnO and 1% to 5% Ce-ZnO NPS

TABLE-2
BAND GAP VALUES FOR SG AND CPPT METHODD FOR PURE AND 1-5% Ce-ZnO NPS

Method	Band gap (eV)					
	ZnO	1% Ce-ZnO	2% Ce-ZnO	3% Ce-ZnO	4% Ce-ZnO	5% Ce-ZnO
Sol-gel	3.13	2.95	2.37	2.86	2.88	2.38
CPPT	3.11	2.84	2.90	2.32	2.36	2.39

and CPPT methods. All samples exhibit characteristic Raman modes of hexagonal wurtzite ZnO. Raman spectrum for 2% and 3% Ce-ZnO for SG and CPPT methods, respectively as shown in Fig. 10. The peaks detected at 336, 385 and 443 cm^{-1} are attributed to the E_2H-E_2L, A1 (TO) and E_2H modes, respectively [37]. The most prominent peak located around 442.09 and 443.90 cm^{-1} (Fig. 10a-b) are associated with the Raman-active E_2H mode that suggests the good crystallinity of the ZnO lattice. A gradual reduction in the intensity and slight broadening shifting of this mode with increasing Ce concentration indicates lattice distortion induced by cerium incorporation (Fig. 10c-d).

Photoluminescence study: The photoluminescence (PL) spectroscopy was used to study charge carrier recombination and defect-related emissions in ZnO and Ce-doped ZnO nanoparticles synthesized by SG and CPPT methods. Each sample shows a near-band-edge (NBE) emission in the ultraviolet region along with a broad visible emission band linked to intrinsic defects. Fig. 11 presents the PL spectra of the photocatalysts which were measured at an excitation wavelength

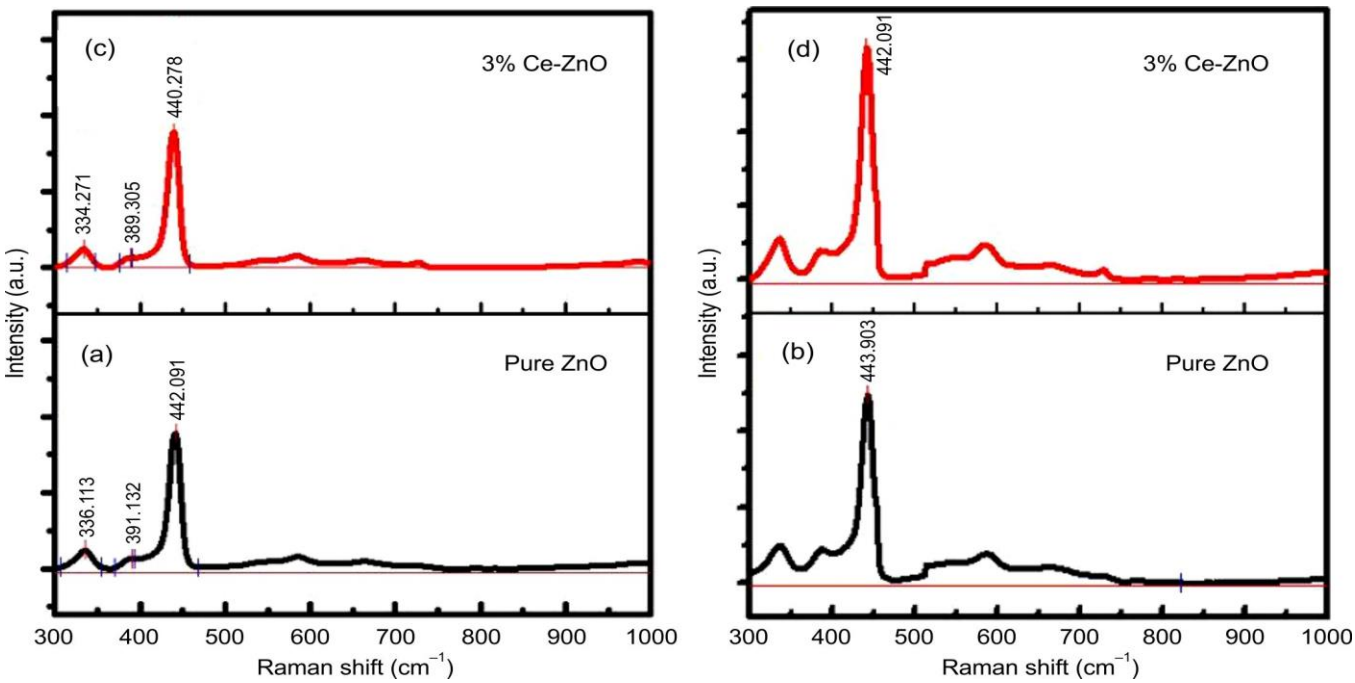

Fig. 10. Raman shift spectrum ZnO by (a) SG (b) CPPT and for 3% Ce-ZnO by (c) SG and (d) CPPT methods

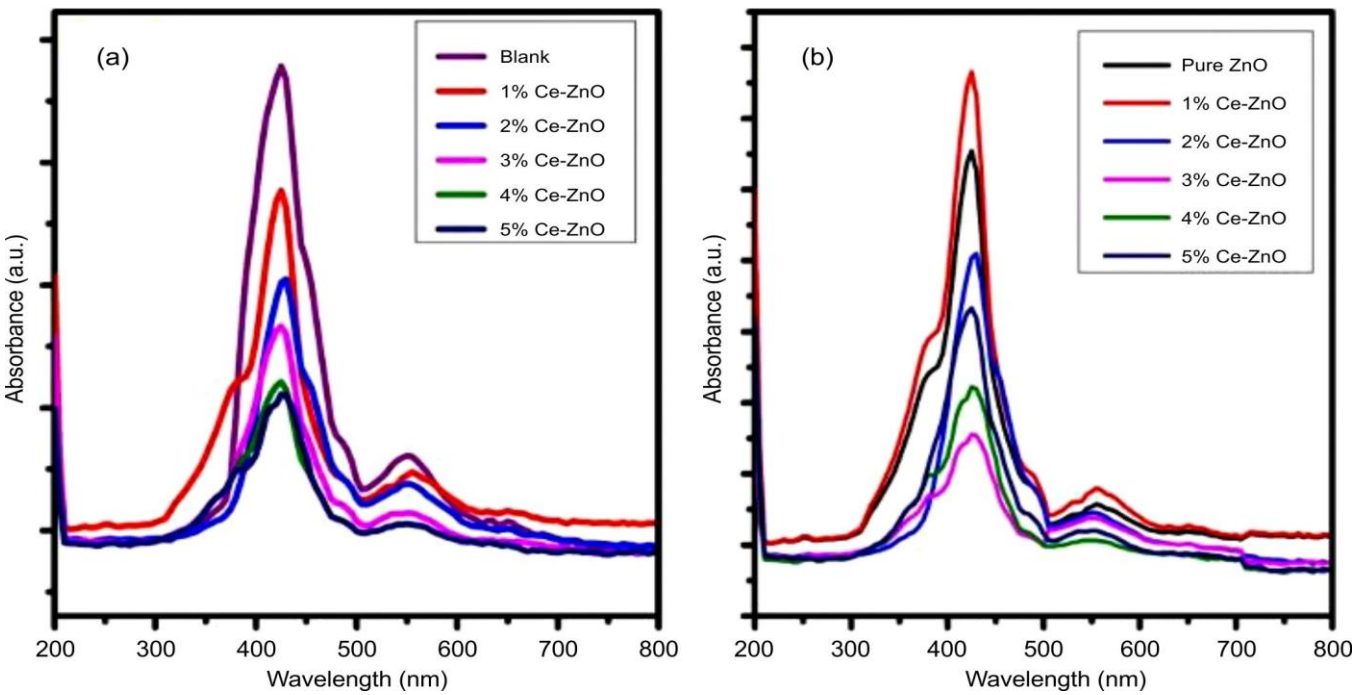

Fig. 11. Photoluminescence spectra for (a) SG and (b) CPPT methods

of 320 nm. The findings indicated that in comparison to ZnO the Ce-doped ZnO did not exhibit any new PL peaks. A peak around 375 nm in the PL spectrum is likely due to free excitonic emission near the absorption edge while the broad and intense emission spectra between 400-600 nm are attributed to defect states in the Ce doped ZnO crystals [47]. The introduction of Ce resulted in a reduction of emission intensities across all samples with the most significant decrease observed at a doping concentration of 2% Ce for SG and 3% Ce for CPPT. This minimal PL emission for the 2% and 3% Ce-doped ZnO photocatalyst implies a significant inhibition of the recombination of photogenerated electrons and holes.

Photocatalytic activity

Degradation of triethylamine: The experiment for photodegradation performance involved subjecting 1500 ppm solutions of triethylamine (m.w. = 101.19 g/mol) and 50 mg of catalyst to visible light in the month of October and time between 11 a.m. to 4 p.m. for 360 min (6 h). That were clear days and light intensity measured by Lux meter corresponding to an estimated irradiance of ~9.175 W/m^2. Before this exposure the prepared catalysts and triethylamine solution were stirred magnetically in the dark for 60 min to reach adsorption–desorption equilibrium. All these tests were performed for without catalyst (as such) and ZnO, 1% to 5% Ce-ZnO prepared by both SG and CPPT method. In these performance, all Ce doped ZnO shows good performance but among all samples, 2% Ce-ZnO for SG and 3% Ce-ZnO for CPPT method showed superior photocatalytic activity compared to ZnO suggesting that the addition of Ce to ZnO enhances its photocatalytic efficiency. Due to ZnO's wide bandgap (3.37 eV), visible light is unable to trigger exciton formation leading to reduced photocatalytic efficiency. The removal of triethylamine in the presence of ZnO is due to the photosensitisation of triethylamine. A higher concentration of Ce leads to the blockage of active sites, reducing photocatalytic activity. Triethylamine shows absorbance at around 215-220 nm in UV-visible spectrum. Figs. 12 and 13a-b shows the UV-Vis spectrum for degradation of triethylamine and (c) shows the percent degradation. Also, the UV spectrum for percent degradation of triethylamine for ZnO and 1% to 5% Ce-ZnO for SG and CPPT method shown in Figs. 14 and 15, respectively. Table-3 shows the comparison between SG and CPPT method for the photocatalytic percent degradation of triethylamine and calculated using following formula:

$$\text{Degradation (\%)} = \frac{C_o - C_t}{C_o} \times 100$$

where C_o is the initial concentration and C_t is the final concentration of the triethylamine.

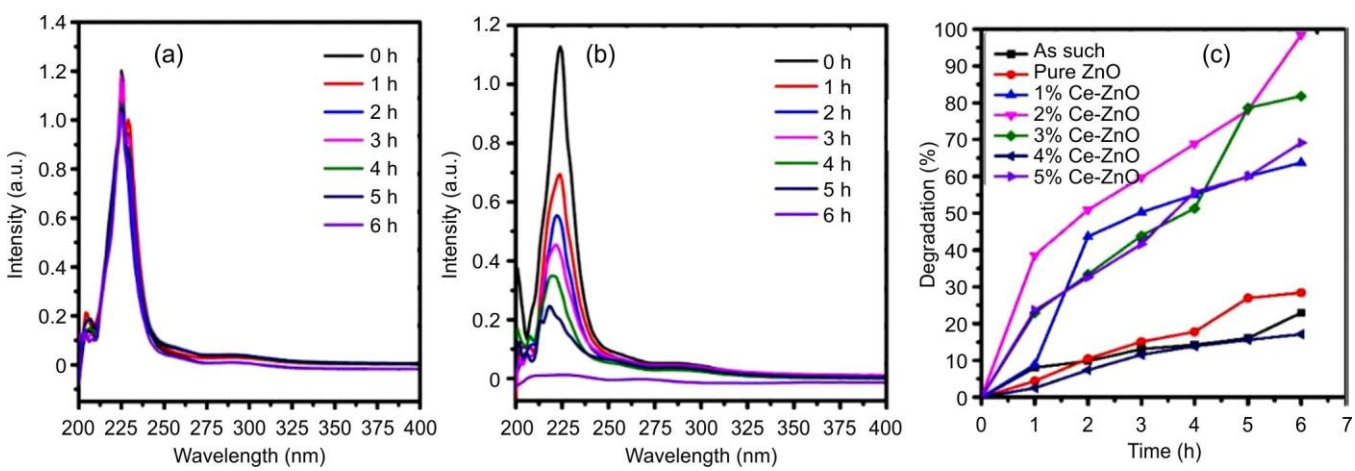

Fig. 12. UV-Vis spectrum for degradation of (a) ZnO (b) 2% Ce-ZnO and (c) % degradation for ZnO and 1% to 5% Ce-ZnO by SG method

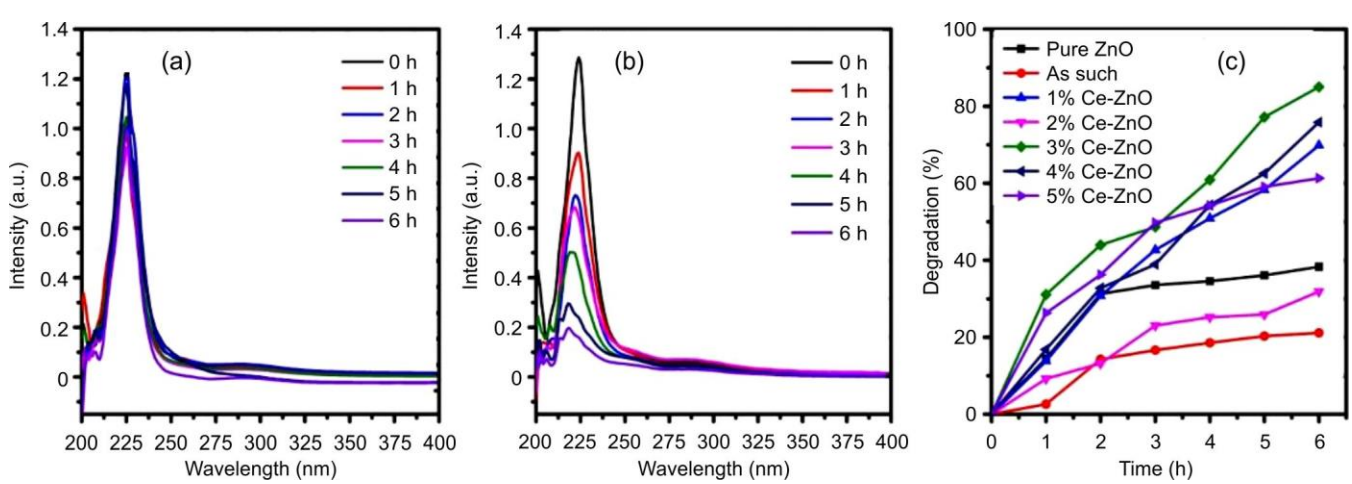

Fig. 13. UV-Vis spectrum for degradation of (a) ZnO (b) 3% Ce-ZnO and (c) % degradation for ZnO and 1% to 5% Ce-ZnO by CPPT method

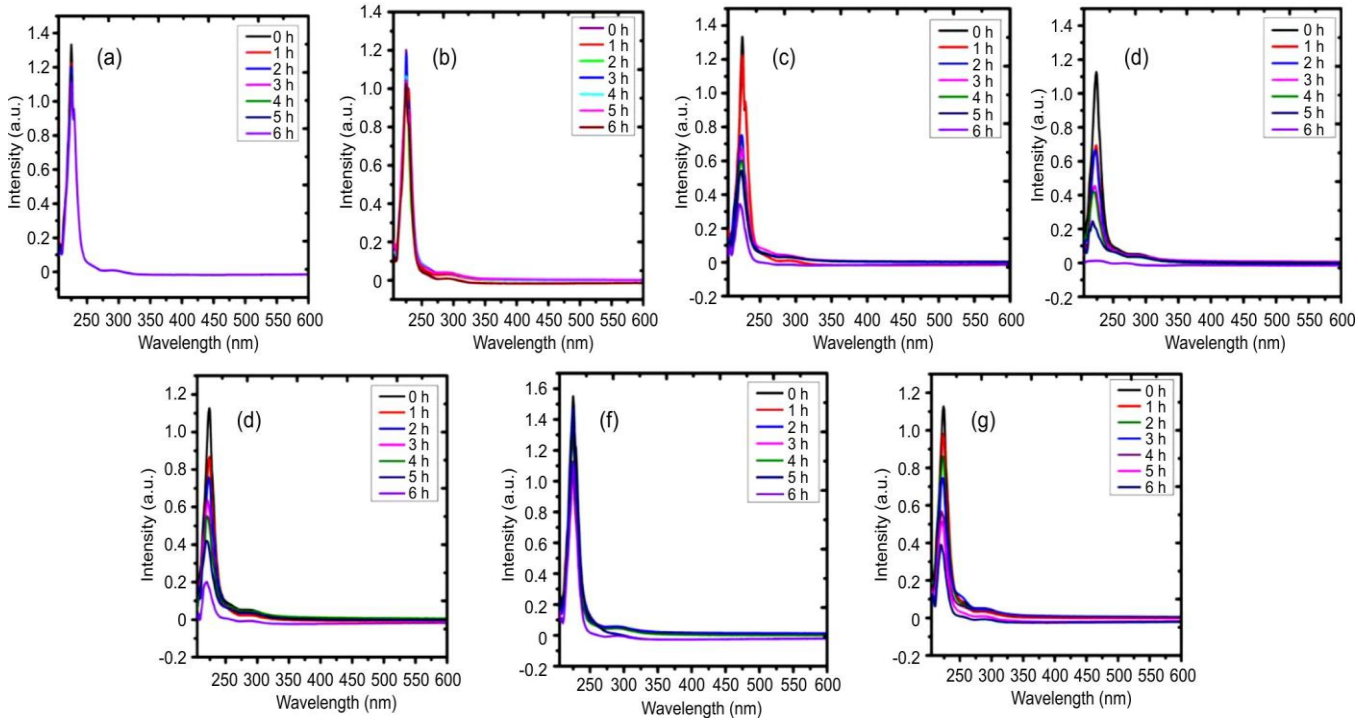

Fig. 14. UV-vis spectrum for degradation of triethylamine using (a) as such (b) pure ZnO (c) 1% (d) 2% (e) 3% (f) 4% and (g) 5% for sol-gel methods

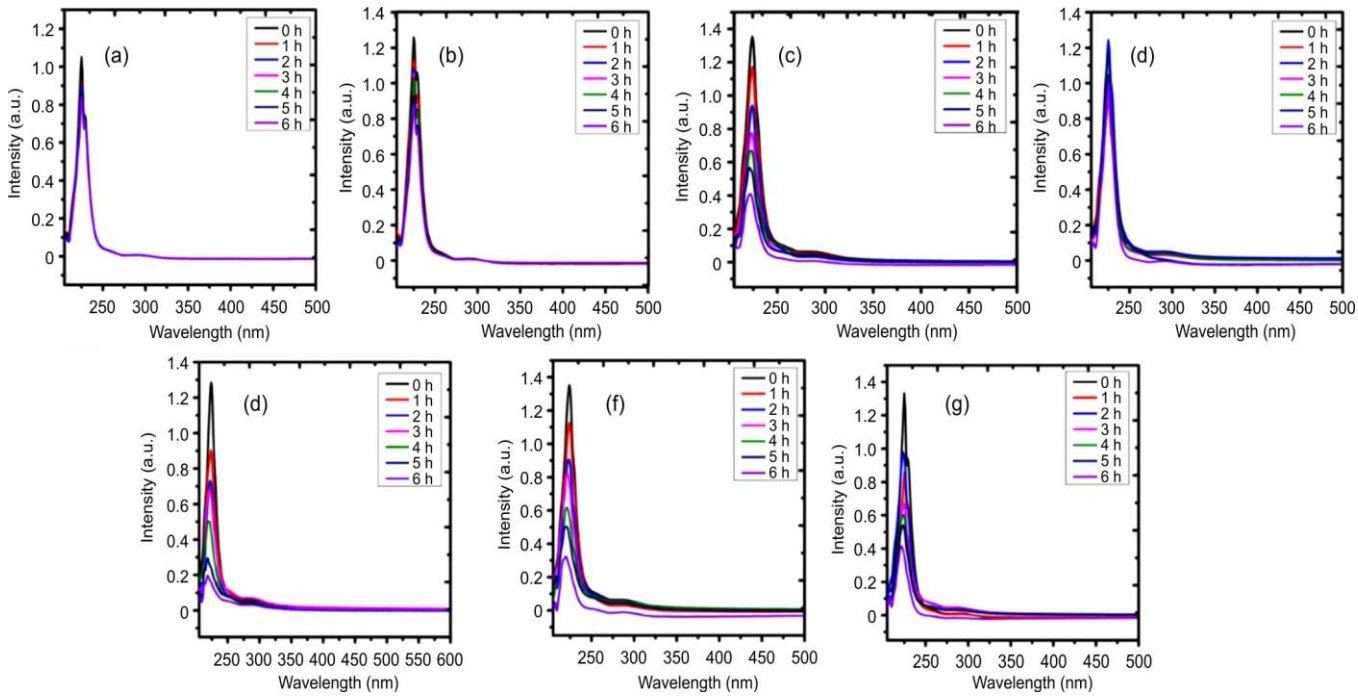

Fig. 15. UV-Vis spectrum for degradation of triethylamine using (a) as such, (b) pure ZnO (c) 1% (d) 2% (e) 3% (f) 4% and (g) 5% for CPPT methods

TABLE-3
COMPARATIVE DEGRADATION OF TEA FOR SG AND CPPT METHODS WITH DIFFERENT CERIUM DOPING

Method	Degradation of triethylamine (%)					
	ZnO	1% Ce-ZnO	2% Ce-ZnO	3% Ce-ZnO	4% Ce-ZnO	5% Ce-ZnO
SG	28.48	63.98	98.12	81.63	16.48	69.21
CPPT	38.31	69.83	31.88	85.01	75.81	61.32

Kinetic studies: The photocatalytic breakdown of triethylamine followed pseudo-first-order kinetics, aligning with the Langmuir-Hinshelwood (L-H) model. The model's linearised equation is given by:

$$\ln\left(\frac{C_o}{C}\right) = kt$$

where C_o and C represent the initial and final concentrations of triethylamine; t denotes the time of irradiation and rate constant is denoted by k.

The 2% Ce-ZnO (k = 0.5366 min^{-1}) and 3% Ce-ZnO (k = 0.2956 min^{-1}) catalysts of SG and CPPT method achieved the highest rate constant, respectively. Catalysts with lower cerium doping exhibited intermediate rate constants (Table-4), which corresponded well with their degradation efficiencies.

TOC analysis: In photocatalytic experiment, samples of the reaction mixture are taken and filtered to separate the catalyst at different times during sunlight irradiation and analysed for TOC on grab mode. A reduction in TOC indicates the degradation of triethylamine results in the formation of CO_2, water and other gases. The TOC of original sample before sunlight irradiation was 935 ppm. The maximum reduction in TOC were observed for 2% Ce-ZnO for SG (117 ppm) and 3% Ce-ZnO for CPPT (192 ppm) method. Typically, the degradation rate of TEA exceeds the rate of TOC reduction, especially at the beginning. This suggests that intermediate organic compounds form before complete mineralisation occurs. With a high initial concentration of 1500 ppm TEA, the slow decrease in TOC with prolonged irradiation high-lights the effectiveness of Ce-ZnO in achieving thorough oxidation. The improved TOC removal compared to undoped ZnO emphasizes the role of cerium in enhancing photocatalytic activity and mineralisation efficiency.

Photocatalytic mechanism: It is widely recognised that when a photocatalyst is exposed to sunlight, it can generate electrons and holes which subsequently migrate to the photocatalyst's surface. These photo-generated electrons and holes engage in a sequence of redox reactions resulting in the formation of hydroxyl radicals that contribute to the breakdown of organic pollutants. Based on the observed photocatalytic performance and degradation products, a possible photocatalytic mechanism is suggested below.

$$\text{Ce-ZnO} + \text{Irradiation} = \text{CB}\ (h^+) + \text{VB}(-e)$$

$$\text{CB}\ (h^+) + H_2O = OH^\bullet$$

$$\text{VB}(-e) + (O_2)\ \text{adsorbed} = O_2$$

$$O_2 + H_2O = OH^\bullet$$

$$OH^\bullet + \text{TEA} = CO_2 + H_2O + NH_3\ \text{(degradation products)}$$

Upon irradiation of the Ce-ZnO composite, electrons are excited from the valence band to the conduction band leaving positive holes in the VB. Ce^+ ions can act as a trap for the photoexcited electrons preventing the recombination of electrons and holes thereby enhancing the photocatalytic activity of Ce-ZnO. The positive holes and electrons generate hydroxyl radicals through a series of reactions which participate in the mineralisation of pollutant TEA. This mechanism is suggested based on literature reports rather than direct *in situ* evidence.

Recycle studies: In a recycling test, the catalyst is retrieved after each photocatalytic cycle using filtration, then cleaned 3 to 4 times with milli-Q water to eliminate any adsorbed intermediates, dried well in oven and reused under the same reaction conditions. The degradation efficiency observed in subsequent cycles helps evaluate the catalyst's structural and functional integrity. In recycle test, the photocatalyst maintains over about 80% of its initial activity over 3 cycles, over that the activity starts decreasing slowly as shown in Fig. 16. This notable decline in performance might suggest catalyst deactivation due to surface poisoning, agglomeration or structural alterations. To observe stability, XRD analysis was also conducted before and after recycling. This shows that there was no any drastic change in their morphology as shown in Fig. 17, which can suggest that the prepared photocatalyst is robust, cost effective and green photocatalyst and can be used for long term for degradation of triethylamine.

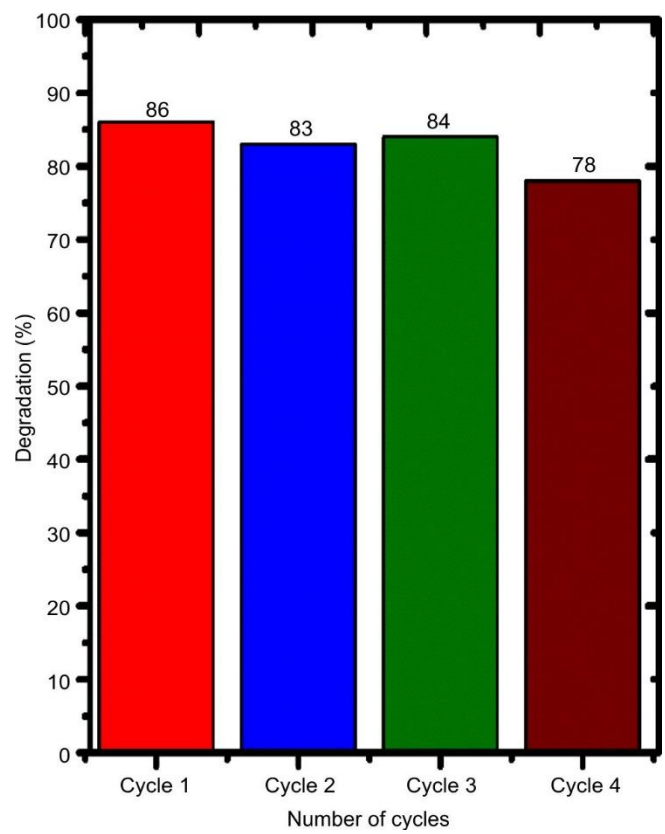

Fig. 16. Recycle study for 2% Ce-ZnO

TABLE-4
RATE CONSTANT FOR DEGRADATION OF TEA FOR SG AND CPPT METHODS

Method	Rate constant (min^{-1})					
	ZnO	1% Ce-ZnO	2% Ce-ZnO	3% Ce-ZnO	4% Ce-ZnO	5% Ce-ZnO
SG	0.0580	0.1756	0.5366	0.2854	0.0330	0.1870
CPPT	0.0415	0.1924	0.0609	0.2952	0.2228	0.1556

TABLE-5
A BRIEF COMPARISON WITH PREVIOUSLY REPORTED Ce-ZnO PHOTOCATALYSTS FOR AMINE OR VOC DEGRADATION

Photocatalyst	Method	Pollutant	Light source	Key results (degradation)	Ref.
Ce-doped ZnO NP's	Sol-gel	Organic pollutants (DB71 dyes)	Incandescent lamp	~96%	[58]
	Coprecipitation	*p*-Xylene (VOC)	Vacuum UV lamp; gas phase	100%	[60]
	Sol gel	Carbamazepine (pharmaceutical amine)	Visible light	~53%	[61]

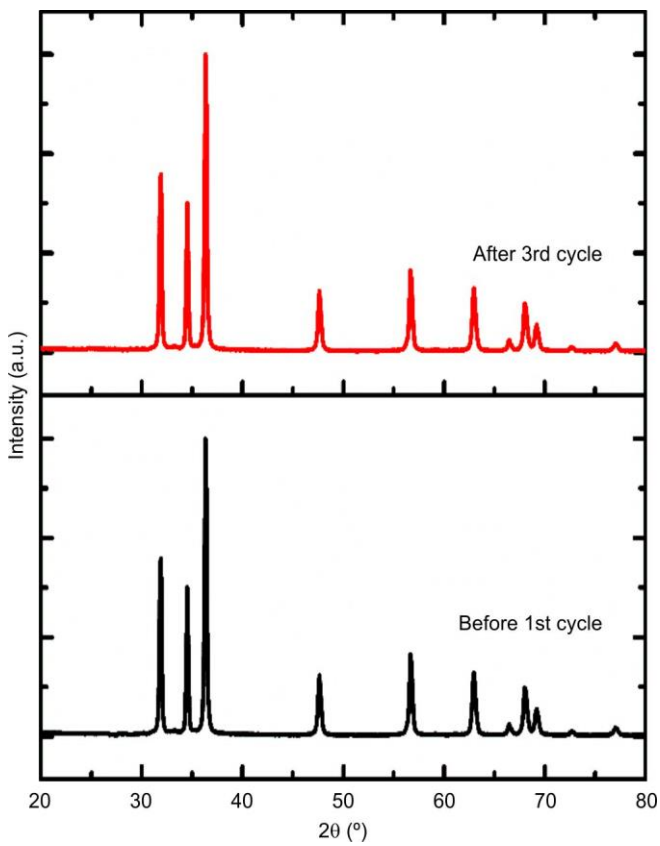

Fig. 17. XRD spectrum of 2% Ce-ZnO before and after recycle study

Comparative studies: Previous researches on Ce-doped ZnO photocatalysts have mainly focused on degradation of volatile organic compounds (VOCs), pharmaceutical pollutants and dyes using artificial UV or visible light using lamp. In this research, however, introduces Ce–ZnO nanoparticles, synthesised through simple and eco-friendly sol-gel and co-precipitation techniques for photodegradation of triethylamine for the first time. Notably, natural sunlight serves as the light source which is easily available, emphasizing a practical and sustainable method. The remarkable degradation rates achieved (94% and 85% for SG and CPPT, respectively) distinguish this study from earlier research. Table-5 indicates a brief comparison with previously reported Ce-ZnO photocatalysts for amine and VOC degradation.

Conclusion

Ce doped ZnO photocatalyst with Ce concentrations ranging from 1-5% were produced through a cost-effective sol-gel and coprecipitation method. These catalysts were evaluated for their ability to degrade triethylamine, a common amine industrial waste under natural sunlight. The doping process led to lattice distortion and narrowing band gap from 3.13 in undoped ZnO to 2.32 eV in the 2% Ce-ZnO (SG) and 2.37 eV for 3% Ce-ZnO (CPPT) samples. Photoluminescence studies indicated that 2% (SG) and 3% (CPPT) Ce doping was most effective in minimizing electron–hole recombination. In photocatalytic experiments, the 2% (SG) and 3% (CPPT) Ce-ZnO catalysts achieved nearly 85-98% degradation of triethylamine within 6 h in natural sunlight. The reaction adhered to the pseudo-first-order kinetics with a rate constant 10-folds (SG) and 7-fold (CPPT) greater than undoped ZnO. The catalyst retained over 85% of its activity after three reuse cycles indicating good stability for solar-driven amine wastewater treatment.

ACKNOWLEDGEMENTS

Special thanks to Annasaheb Magar College, Pune, India for providing the necessary resources and research facilities.

CONFLICT OF INTEREST

The authors declare that there is no conflict of interests regarding the publication of this article.

DECLARATION OF AI-ASSISTED TECHNOLOGIES

During the preparation of this manuscript, the authors used an AI-assisted tool(s) to improve the language. The authors reviewed and edited the content and take full responsibility for the published work.

REFERENCES

1. N. Roy, N.T. Paira and R. Chakrabarty, *RSC Adv.*, **15**, 3008 (2025); https://doi.org/10.1039/D4RA07604D
2. R. Al-Tohamy, S.S. Ali, F. Li, K.M. Okasha, Y.A.-G. Mahmoud, T. Elsamahy, H. Jiao, Y. Fu and J. Sun, *Ecotoxicol. Environ. Saf.*, **231**, 113160 (2022); https://doi.org/10.1016/j.ecoenv.2021.113160
3. S.H. Safaei and S. Young, *Carbon Capture Sci. Technol.*, **16**, 100475 (2025); https://doi.org/10.1016/j.ccst.2025.100475
4. P. Pankaj, M. Verma, S. Goyal and P.K. Patnala, *Mater. Sci. Forum*, 712, 147 (2012); https://doi.org/10.4028/www.scientific.net/MSF.712.147
5. J. Nanthakumar, Y. Palanisamy, S. Palanisamy, M. Karuppusamy, R. Raja, M. Abbas, A. Alagarsamy and M.Z. Rahman, *RSC Adv.*, **15**, 39305 (2025); https://doi.org/10.1039/D5RA05208D
6. B. Ben Salem, W. Ltaief, S. Ben Ameur, H. Guermazi, S. Guermazi, B. Duponchel and G. Leroy, *RSC Adv.*, **15**, 13825 (2025); https://doi.org/10.1039/D5RA00756A
7. F.T.Z. Toma, M.S. Rahman and K.H. Maria, *Discov. Mater.*, **5**, 60 (2025); https://doi.org/10.1007/s43939-025-00201-1

8. M. Swain, D. Mishra and G. Sahoo, *Discover. Appl. Sci.*, **7**, 997 (2025); https://doi.org/10.1007/s42452-025-06957-8
9. B. Anchan, S. Kamath U, S.D. Kulkarni, K.A. Pandey, S. De and A. Patil, *Sci. Rep.*, **15**, 11219 (2025); https://doi.org/10.1038/s41598-025-95892-0
10. Y. Xie, B. Yan, H. Xu, J. Chen, Q. Liu, Y. Deng and H. Zeng, *ACS Appl. Mater. Interfaces*, **6**, 8845 (2014); https://doi.org/10.1021/am501632f
11. H. Qian, J. Wang and L. Yan, *J. Bioresour. Bioprod.*, **5**, 204 (2020); https://doi.org/10.1016/j.jobab.2020.07.006
12. W. Ouyang, S. Liu, K. yao, L. Zhao, L. Cao, S. Jiang and H. Hou, *Compos. Commun.*, **9**, 76 (2018); https://doi.org/10.1016/j.coco.2018.06.006
13. B. Subash, B. Krishnakumar, R. Velmurugan, M. Swaminathan and M. Shanthi, *Catal. Sci. Technol.*, **2**, 2319 (2012); https://doi.org/10.1039/c2cy20254a
14. W. Xue, G. Zhang, X. Xu, X. Yang, C. Liu and Y. Xu, *Chem. Eng. J.*, **167**, 397 (2011); https://doi.org/10.1016/j.cej.2011.01.007
15. J. Shao, Y. Ni and L. Yan, *J. Bioresour. Bioprod.*, **6**, 39 (2021); https://doi.org/10.1016/j.jobab.2021.02.005
16. S.K. Fanourakis, J. Peña-Bahamonde, P.C. Bandara and D.F. Rodrigues, *NPJ Clean Water*, **3**, 1 (2020); https://doi.org/10.1038/s41545-019-0048-8.
17. Q. Gao, L. Bao, H. Mao, L. Wang, K. Xu, M. Yang, Y. Li, L. Zhu, N. Wang, Z. Lv, H. Gao, X. Ge, B. Kan, Y. Hu, J. Liu, F. Cai, D. Jiang, Y. Yin, C. Qin, J. Li, X. Gong, X. Lou, W. Shi, D. Wu, H. Zhang, L. Zhu, W. Deng, Y. Li, J. Lu, C. Li, X. Wang, W. Yin, Y. Zhang and C. Qin, *Science*, **369**, 77 (2020); https://doi.org/10.1126/science.abc1932
18. H. Tong, S. Ouyang, Y. Bi, N. Umezawa, M. Oshikiri and J. Ye, *Adv. Mater.*, **24**, 229 (2012); https://doi.org/10.1002/adma.201102752
19. M. Khan, B. Ahmad, K. Hayat, F. Ullah, N. Sfina, M. Elhadi, A.A. Khan, M. Husain and N. Rahman, *RSC Adv.*, **14**, 2402 (2024); https://doi.org/10.1039/D3RA07441B
20. N. Narayanan and N.K. Deepak, *Solid State Sci.*, **78**, 144 (2018); https://doi.org/10.1016/j.solidstatesciences.2018.02.017
21. C. Jayachandraiah and G. Krishnaiah, *J. Mater. Sci.*, **52**, 7058 (2017); https://doi.org/10.1007/s10853-017-0938-4
22. H. Akhtar, F.H. Alhamoudi, J. Marshall, T. Ashton, J.A. Darr, I.U. Rehman, A.A. Chaudhry and G. Reilly, *Heliyon*, **10**, e29150 (2024); https://doi.org/10.1016/j.heliyon.2024.e29150
23. X. Li, J. Li, S. Li, X. Fang, F. Fang, X. Chu, X. Wang and J. Hu, *Chem. Res. Chin. Univ.*, **29**, 1032 (2013); https://doi.org/10.1007/s40242-013-3354-6
24. A. Kumawat, A. Sharma, S. Chattopadhyay and K.P. Misra, *Mater. Today Proc.*, **43**, 2965 (2021); https://doi.org/10.1016/j.matpr.2021.01.322
25. O. Yayapao, S. Thongtem, A. Phuruangrat and T. Thongtem, *Ceram. Int.*, **39**, S563 (2013); https://doi.org/10.1016/j.ceramint.2012.10.136
26. A. Hezam, K. Namratha, Q.A. Drmosh, Z.H. Yamani and K. Byrappa, *Ceram. Int.*, **43**, 5292 (2017); https://doi.org/10.1016/j.ceramint.2017.01.059
27. R. Saravanan, H. Shankar, T. Prakash, V. Narayanan and A. Stephen, *Mater. Chem. Phys.*, **125**, 277 (2011); https://doi.org/10.1016/j.matchemphys.2010.09.030
28. W. Guo and H. Liu, *Chem. Res. Chin. Univ.*, **33**, 129 (2017); https://doi.org/10.1007/s40242-017-6098-x
29. O. Długosz and M. Banach, *J. Nanostruct. Chem.*, **11**, 601 (2021); https://doi.org/10.1007/s40097-021-00387-9
30. R. Guan, H. Zhai, D. Sun, J. Zhang, Y. Wang and J. Li, *Chem. Res. Chin. Univ.*, **35**, 271 (2019); https://doi.org/10.1007/s40242-019-8275-6
31. U. Alam, A. Khan, W. Raza, A. Khan, D. Bahnemann and M. Muneer, *Catal. Today*, **284**, 169 (2017); https://doi.org/10.1016/j.cattod.2016.11.037
32. W. Liang, B.D. Yuhas and P. Yang, *Nano Lett.*, **9**, 892 (2009); https://doi.org/10.1021/nl8038184
33. S.H. Kim, A. Umar, Y.K. Park, J.-H. Kim, E.W. Lee and Y.B. Hahn, *J. Alloys Compd.*, **479**, 290 (2009); https://doi.org/10.1016/j.jallcom.2008.11.106
34. J. Jie, G. Wang, X. Han, Q. Yu, Y. Liao, G. Li and J.G. Hou, *Chem. Phys. Lett.*, **387**, 466 (2004); https://doi.org/10.1016/j.cplett.2004.02.045
35. A.A. Ibrahim, G.N. Dar, S.A. Zaidi, A. Umar, M. Abaker, H. Bouzid and S. Baskoutas, *Talanta*, **93**, 257 (2012); https://doi.org/10.1016/j.talanta.2012.02.030
36. A. Khataee, S. Saadi and B. Vahid, *Ultrason. Sonochem.*, **34**, 98 (2017); https://doi.org/10.1016/j.ultsonch.2016.05.026
37. R. Al Abri, F. Al Marzouqi, A.T. Kuvarega, M.A. Meetani, S.M.Z. Al Kindy, S. Karthikeyan, Y. Kim and R. Selvaraj, *J. Photochem. Photobiol. Chem.*, **384**, 112065 (2019); https://doi.org/10.1016/j.jphotochem.2019.112065
38. L. Wang, Z. Ji, J. Lin and P. Li, *Mater. Sci. Semicond. Process.*, **71**, 401 (2017); https://doi.org/10.1016/j.mssp.2017.09.001
39. S.P. Meshram, P.V. Adhyapak, S.K. Pardeshi, I.S. Mulla and D.P. Amalnerkar, *Powder Technol.*, **318**, 120 (2017); https://doi.org/10.1016/j.powtec.2017.05.044
40. N.C. Birben, M.C. Paganini, P. Calza and M. Bekbolet, *Photochem. Photobiol. Sci.*, **16**, 24 (2017); https://doi.org/10.1039/c6pp00216a
41. G. Duan, H. Fang, C. Huang, S. Jiang and H. Hou, *J. Mater. Sci.*, **53**, 15096 (2018); https://doi.org/10.1007/s10853-018-2700-y
42. Y. Wang, W. Li, S. Chao, Y. Li, X. Li, D. He and C. Wang, *Chem. Res. Chin. Univ.*, **36**, 1292 (2020); https://doi.org/10.1007/s40242-020-0215-y
43. S. Jiang, J.Y. Cheong, J.S. Nam, I.-D. Kim, S. Agarwal and A. Greiner, *ACS Appl. Mater. Interfaces*, **12**, 19006 (2020); https://doi.org/10.1021/acsami.0c02004
44. S. Zhou, G. Zhou, S. Jiang, P. Fan and H. Hou, *Mater. Lett.*, **200**, 97 (2017); https://doi.org/10.1016/j.matlet.2017.04.115
45. L. Zhang, D. Austin, V.I. Merkulov, A.V. Meleshko, K.L. Klein, M.A. Guillorn, D.H. Lowndes and M.L. Simpson, *Appl. Phys. Lett.*, **84**, 3972 (2004); https://doi.org/10.1063/1.1748849
46. J. Liu, J. Li, A. Sedhain, J. Lin and H. Jiang, *J. Phys. Chem. C*, **112**, 17127 (2008); https://doi.org/10.1021/jp8060653
47. M. Ahmad, E. Ahmed, F. Zafar, N.R. Khalid, N.A. Niaz, A. Hafeez, M. Ikram, M.A. Khan and Z. Hong, *J. Rare Earths*, **33**, 255 (2015); https://doi.org/10.1016/S1002-0721(14)60412-9
48. S.D. Wakade and V.T. Vader, *Discover Chem.*, **2**, 114 (2025); https://doi.org/10.1007/s44371-025-00196-x
49. A.K. Dhanka, B. Pani and N. Agasti, *RSC Adv.*, **15**, 11774 (2025); https://doi.org/10.1039/D5RA00640F
50. M. Tashakkori Masuleh, M. Hasheminiasari and R. Ashiri, *Mater. Adv.*, **6**, 2611 (2025); https://doi.org/10.1039/D5MA00026B
51. J. Yang, M. Gao, L. Yang, Y. Zhang, J. Lang, D. Wang, Y. Wang, H. Liu and H. Fan, *Appl. Surf. Sci.*, **255**, 2646 (2008); https://doi.org/10.1016/j.apsusc.2008.08.001
52. A.B. Moghaddam, T. Nazari, J. Badraghi and M. Kazemzad, *Int. J. Electrochem. Sci.*, **4**, 247 (2009); https://doi.org/10.1016/S1452-3981(23)15125-X
53. H. Parangusan, D. Ponnamma and M.A.A. Al-Maadeed, *Bull. Mater. Sci.*, **42**, 179 (2019); https://doi.org/10.1007/s12034-019-1865-6

54. T.K. Pathak, E. Coetsee-Hugo, H.C. Swart, C.W. Swart and R.E. Kroon, *Mater. Sci. Eng. B*, **261**, 114780 (2020); https://doi.org/10.1016/j.mseb.2020.114780
55. C.R. Brundle and R.I. Bickley, *J. Chem. Soc., Faraday Trans. II*, **75**, 1030 (1979); https://doi.org/10.1039/f29797501030
56. M. Yousefi, M. Amiri, R. Azimirad and A.Z. Moshfegh, *J. Electroanal. Chem.*, **661**, 106 (2011); https://doi.org/10.1016/j.jelechem.2011.07.022
57. M. Faisal, A.A. Ismail, A.A. Ibrahim, H. Bouzid and S.A. Al-Sayari, *Chem. Eng. J.*, **229**, 225 (2013); https://doi.org/10.1016/j.cej.2013.06.004
58. D.T.B. Hop, T.Q. Tuan, N.V. Quang, N. Tu, H.L. Tien, M.T. Tran, T.Q. Vinh, N.C. Tu, T.N. Bach, V.-D. Dao and P.T.L. Huong, *Ceram. Int.*, **50**, 17338 (2024); https://doi.org/10.1016/j.ceramint.2024.02.216
59. T.V. Ha Luu, T.L. Nguyen, T.M. Hien Bach, N.T. Dung, N.N. Huy and H.P. Dang, *RSC Adv.*, **15**, 26552 (2025); https://doi.org/10.1039/D5RA03520A
60. Z. Cheng, J. Wang, D. Chen, J. Yu, S. Zhang, S. Wang and Y. Dai, *Catal. Sci. Technol.*, **11**, 612 (2021); https://doi.org/10.1039/D0CY01140A
61. P. Caregnato, K.R. Espinosa Jiménez and P.I. Villabrille, *Catal. Today*, **372**, 183 (2021); https://doi.org/10.1016/j.cattod.2020.07.031